Monthly Notices
of the
ROYAL ASTRONOMICAL SOCIETY

MNRAS **465,** 1601–1607 (2017)
Advance Access publication 2016 November 10

doi:10.1093/mnras/stw2886

A high-precision polarimeter for small telescopes

Jeremy Bailey,[1,2]★ Daniel V. Cotton[1,2] and Lucyna Kedziora-Chudczer[1,2]

[1]*School of Physics, UNSW Australia, Sydney, NSW 2052, Australia*
[2]*Australian Centre for Astrobiology, UNSW Australia, Sydney, NSW 2052, Australia*

Accepted 2016 November 4. Received 2016 November 4; in original form 2016 October 4

ABSTRACT

We describe Mini-HIPPI (Miniature HIgh Precision Polarimetric Instrument), a stellar polarimeter weighing just 650 gm but capable of measuring linear polarization to $\sim 10^{-5}$. Mini-HIPPI is based on the use of a Ferroelectric Liquid Crystal modulator. It can easily be mounted on a small telescope and allows us to study the polarization of bright stars at levels of precision which are hitherto largely unexplored. We present results obtained with Mini-HIPPI on a 35-cm telescope. Measurements of polarized standard stars are in good agreement with predicted values. Measurements of a number of bright stars agree well with those from other high-sensitivity polarimeters. Observations of the binary system Spica show polarization variability around the orbital cycle.

Key words: polarization – instrumentation: polarimeters – techniques: polarimetric.

1 INTRODUCTION

Recently, a number of polarimeters have been developed that can measure stellar polarization at parts-per-million (ppm) levels (Hough et al. 2006; Wiktorowicz & Matthews 2008; Bailey et al. 2015; Wiktorowicz & Nofi 2015). All of these instruments are on 3–5 m class telescopes, and one of their main aims has been the measurement of polarized reflected light from extrasolar planets (e.g. Lucas et al. 2009; Wiktorowicz et al. 2015; Bott et al. 2016). However, such instruments can also provide valuable data on the polarization of bright stars. For example, surveys of bright stars (Bailey, Lucas & Hough 2010; Cotton et al. 2016a) have identified interstellar polarization in relatively nearby stars, and found that intrinsic polarization in normal stars is more common than had previously been thought. For studies of the polarization of bright stars, it is not necessary to use a telescope as large as 3–5 m.

Most of these instruments have been based on the photoelastic modulator technology originally developed by James Kemp (Kemp 1969; Kemp & Barbour 1981; Kemp et al. 1987). However, Bailey et al. (2015) showed that high polarimetric sensitivity could also be achieved using ferroelectric liquid crystal (FLC) modulators. The compact size and simple drive requirements of FLCs make them ideally suited to the development of extremely small and lightweight instruments. Here, we describe an FLC-based polarimeter sufficiently compact and lightweight to be mounted on even the smallest telescopes.

★ E-mail: j.bailey@unsw.edu.au

2 INSTRUMENT DESCRIPTION

2.1 Overview

Mini-HIPPI is based on the same design principles as the HIPPI instrument (Bailey et al. 2015) used on the 3.9-m Anglo-Australian Telescope (AAT). HIPPI was commissioned in 2014 and has been used regularly on the AAT for a number of applications (Bailey et al. 2015; Cotton et al. 2016a; Bott et al. 2016; Marshall et al. 2016). Mini-HIPPI shares the same modulators, detectors, and data acquisition and data reduction software.

The optical system of Mini-HIPPI is shown in Fig. 1, and a picture of the instrument is given in Fig. 2.

In order of their position on the light path from the telescope, the components of the instrument are as follows:

(i) A Thorlabs PRM1Z8 motorized rotation stage allows the whole instrument to be rotated.

(ii) The first optical element is the FLC modulator. This is an LV1300-AR-OEM device from Micron Technology. It is designed for the 400–700 nm wavelength range. It operates as an electrically switched half-wave plate driven by a ±5 V square wave, which causes the optical axis to switch between two orientations 45° apart. The normal modulation frequency used is 500 Hz. Further details on these devices and the method of driving them can be found in Bailey et al. (2015). The FLC is a temperature-sensitive device and is therefore mounted in a temperature-controlled lens tube (Thorlabs SM1L10H) and maintained at a temperature of 25°C.

(iii) Behind the lens tube carrying the FLC is a rotatable backend module that carries the aperture, polarizing prism and detectors. This can be adjusted in rotation to minimize the instrumental polarization, as described below. The aperture is mounted on a removable slide to allow change of aperture sizes.

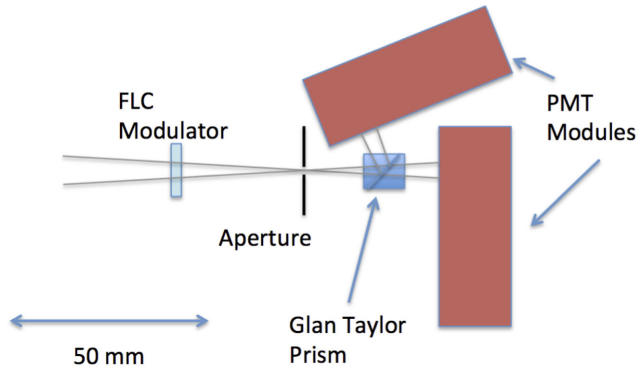

Figure 1. Optical system of Mini-HIPPI.

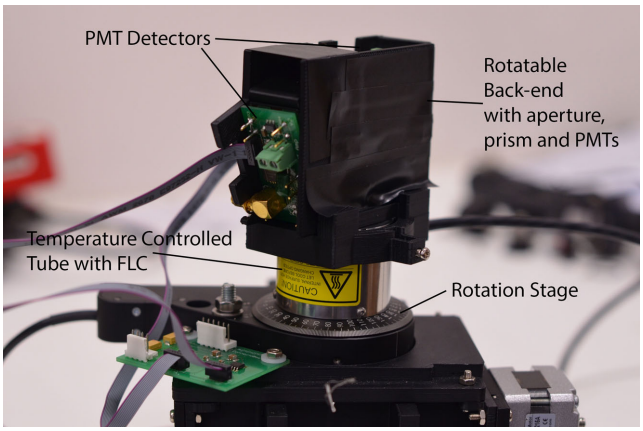

Figure 2. Mini-HIPPI with the main components indicated.

(iv) The polarizing prism is a calcite Glan–Taylor prism (Thorlabs GT5-A) of 5-mm aperture. This splits the light into two beams with orthogonal polarizations, one passing straight through the prism and the other directed upwards at an angle of 68° to the incident beam.

(v) The two beams are fed into two Hamamatsu H10720-210 Photomultiplier Tube (PMT) modules with attached transimpedance amplifiers, identical to those used with HIPPI (Bailey et al. 2015).

Apart from the commercial components described above, the construction of the instrument is entirely by 3D printing in black acrylonitrile butadiene styrene plastic.

The main differences from HIPPI are as follows:

(i) *Use of a Glan–Taylor prism rather than a Wollaston prism*. This makes possible a much shorter light path helping to keep the instrument compact.

(ii) *Lack of any lenses*. HIPPI used lenses to collimate the beam through the prism, and Fabry lenses to image the pupil on to the detectors. The extremely short light path in Mini-HIPPI allows the diverging beam from the aperture to be fed straight into the detectors while still being well within the 8 mm diameter of the photocathodes.

(iii) *Lack of a motorized back-end rotation*. This means that Mini-HIPPI only has two stages of modulation (primary FLC 500 Hz modulation and the whole instrument rotation), whereas HIPPI has three.

(iv) *Mini-HIPPI does not have a filter wheel*. It has been designed to allow a fixed 25-mm-diameter filter to be fitted, but we normally use Mini-HIPPI without a filter, giving a broad bandpass defined mostly by the PMT response. This helps to maximize the signal with small telescopes.

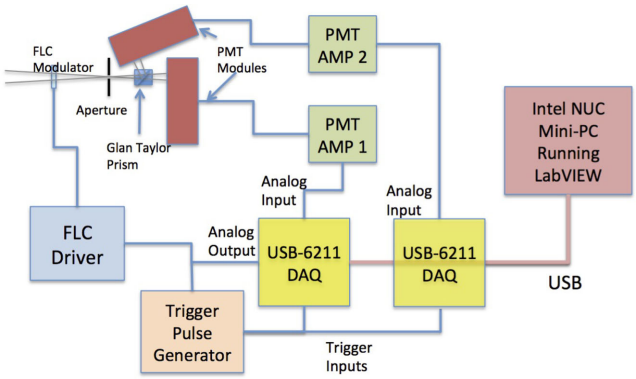

Figure 3. Mini-HIPPI data acquisition and control system.

While all the observations described here use blue-sensitive PMTs and a modulator optimized for blue wavelengths, it is relatively straightforward to adapt the instrument for red wavelengths by fitting a red-optimized FLC modulator and red-sensitive Hamamatsu H10720-20 PMT modules with extended red multi-alkali photocathodes sensitive out to 920 nm.

2.2 Data acquisition system

The data acquisition system for mini-HIPPI (see Fig. 3) is similar to that for HIPPI and uses essentially the same software developed in the National Instruments LabVIEW graphical programming environment. However, the control electronics has been made more compact by using an Intel NUC miniature PC, running Windows 7 Professional and connected to two National Instruments USB-6211 data acquisition modules. These provide analog inputs to read the signals from the PMTs and analog outputs to provide the drive waveform to the FLC modulator as well as the control signals to set the PMT gain and high-tension (HT) voltage.

In operation, the signals are read at a 10 μs sample time, synchronized with the modulation using a trigger pulse derived from the FLC drive waveform. The signals are folded over the modulation period (2 ms for our standard 500 Hz modulation frequency) and written to output files after an integration time of typically 1 s. The format of the output files is identical to those written by HIPPI and can be analysed using the same data reduction software.

A simple quick-look data reduction system built into the acquisition software allows polarization levels to be assessed in real time.

2.3 Observing procedure

As explained by Bailey et al. (2015), polarimeters of this design inherently have a substantial instrumental polarization due to multiple reflection effects in the FLC modulator (Gisler, Feller & Gandorfer 2003; de Juan Ovelar et al. 2012). The key to achieving high precision is designing the instrument in a way that this instrumental polarization can be removed. This is possible because the instrument measures only one Stokes parameter at a time. By rotating the back-end of the instrument relative to the FLC, a one-time adjustment when the instrument is set up, a setting can be found at which the instrumental polarization is orthogonal to the Stokes parameter being measured. This reduces the instrumental polarization to around 100 ppm or less.

This residual instrumental polarization is then eliminated by repeating all observations with the whole instrument rotated through 90° relative to the telescope and sky. This reverses the measured sign of any real polarization while leaving the instrumental polarization unchanged. In practice, we observe at four position angles (0°, 45°, 90° and 135°). One Stokes parameter is obtained from the 0° and 90° observations, and the other from the 45° and 135° observations.

These measured polarizations will still include any polarization introduced by the telescope (telescope polarization or TP). This must be corrected by observations of low-polarization stars, as described later.

2.4 Data reduction

The data reduction software used for Mini-HIPPI is identical to that for HIPPI described in Bailey et al. (2015). The polarization is determined by fitting a modelled curve to the observed modulation waveforms using a Mueller matrix model of the instrument. The Mueller matrix for the instrument is the matrix $\mathbf{M}$ that transforms the input Stokes vector of the source being observed $\boldsymbol{s}_{\mathbf{in}}$ with components (I, Q, U, V) into the output Stokes vector $\boldsymbol{s}_{\mathbf{out}}$ seen at the detector:

$$\boldsymbol{s}_{\mathbf{out}} = \mathbf{M}\boldsymbol{s}_{\mathbf{in}}. \quad (1)$$

The matrix $\mathbf{M}$ is itself the product of the Mueller matrices for each of the optical elements in the system as follows:

$$\mathbf{M} = \mathbf{M}_{\mathrm{Pol}}\mathbf{M}_{\mathrm{Ret}}\mathbf{M}_{\mathrm{Depol}}, \quad (2)$$

where $\mathbf{M}_{\mathrm{Pol}}$ describes the polarizing effect of the Glan-Taylor prism, $\mathbf{M}_{\mathrm{Ret}}$ describes the retardance of the modulator, and $\mathbf{M}_{\mathrm{Depol}}$ describes the depolarizing effect of the modulator. The matrix $\mathbf{M}$ varies around the modulation cycle because the retardance and depolarization vary. We can determine the form of this variation by a laboratory calibration procedure where known polarization states are input to the instrument using a lamp and rotatable polarizer. From the set of matrices $\mathbf{M}$ at different modulation phases, we can then define a system matrix $\mathbf{W}$ which when multiplied by the input Stokes vector gives the observed vector of output intensities at each modulation phase. From the inverse of this matrix (Sabatke et al. 2000), we can then derive the input polarization from the observed modulation curve. Full details of this procedure are given in Bailey et al. (2015).

2.5 Bandpass model

Mini-HIPPI is normally used without a filter and therefore has a broad spectral response from around 350–700 nm but with the peak in the blue at around 440 nm due to the response of the ultra-bialkali photocathodes used. This broad response means that the precise effective wavelength depends on the colour of the object being observed. The modulation efficiency of the polarimeter is also wavelength-dependent. The FLC modulators used are designed to be half-wave plates at about 500 nm. The modulation efficiency falls off at wavelengths either side of this.

To account for these effects, we use a bandpass model as described in Bailey et al. (2015). This model allows us to specify a source spectrum, usually one of the stellar atmosphere models from Castelli & Kurucz (2004), optionally correct it for interstellar extinction, and then apply atmospheric transmission and instrument response functions to allow determination of the effective wavelength, and bandpass averaged modulation efficiency. The typical results for nearby stars (no interstellar extinction) are given in Table 1. Examples of response curves are given in Fig. 4.

Table 1. Effective wavelength and modulation efficiency for different spectral types according to bandpass model.

Spectral type	Effective wavelength (nm)	Modulation efficiency (%)
B0 V	438.7	69.2
A0 V	458.2	78.8
F0 V	467.5	80.4
G0 V	478.2	82.2
K0 V	490.3	85.0
M0 V	509.9	86.6
M5 V	510.4	86.2

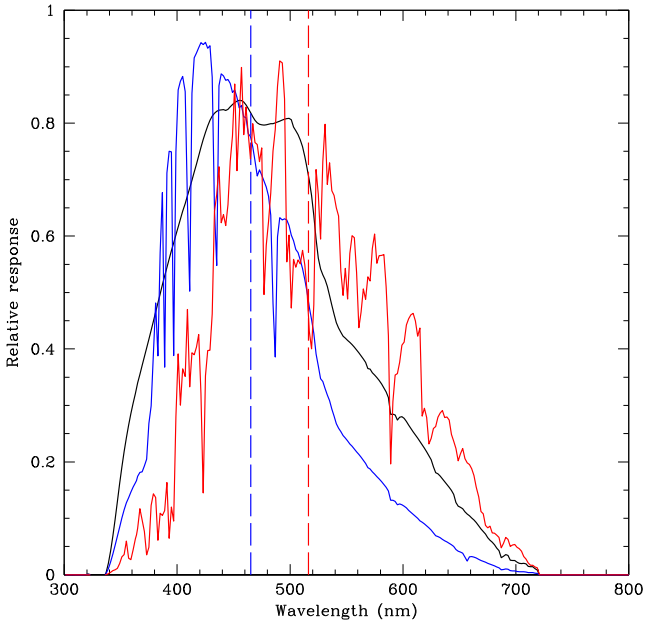

Figure 4. The black line is the instrument response of Mini-HIPPI obtained by combining the atmospheric and instrument throughput and the response of the PMT detector. The blue and red curves show the effective response when observing an A0 star and an M0 star (using Kurucz model spectra). The dashed lines show the effective wavelength in each case, which shifts from 458.2 nm for the A0 to 509.9 nm for the M0 star. See also Table 1.

3 OBSERVATIONS

The observations described here were used to test and evaluate Mini-HIPPI and were made at the UNSW Observatory located at the Kesington campus in Sydney. The telescope is a 35-cm Schmidt Cassegrain (Celestron-14) mounted on a Losmandy German Equatorial mount. We attached Mini-HIPPI to the telescope via an acquisition module that allowed the field of view to be imaged via a flip-in mirror, which can then be removed to pass the starlight through to the instrument. The weight of the instrument plus acquisition module is 1.2 kg. It attaches to the telescope through a standard 2-in. eyepiece fitting. The instrument mounted on the telescope is shown in Fig. 5. A camera mounted on an attached 80-mm guide telescope is used for field acquisition and autoguiding.

The focal length of the telescope is 3900 mm, and our 1.2-mm aperture corresponds to 63 arcsec on the sky. With this large aperture and our city site, which is never really dark even when the Moon is absent, it is important to correct for sky background. Each observation consists of measurements at four rotator position angles, and at each of these angles, we also make at least one sky observation. For long integrations on fainter targets we take sky measurements

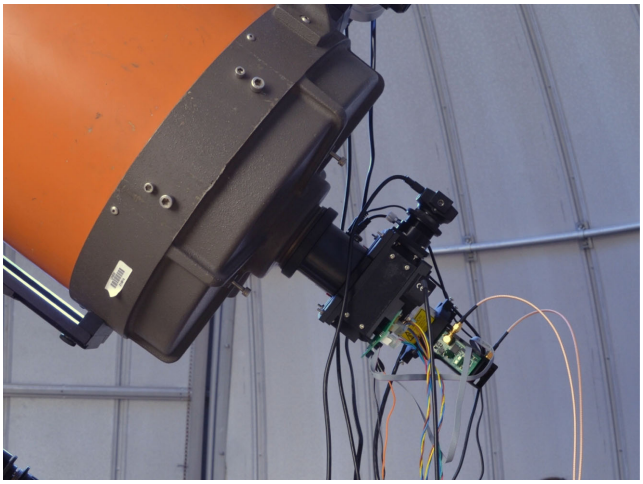

Figure 5. Mini-HIPPI mounted on the 35-cm telescope at the UNSW Observatory.

before and after the target observations at each angle. The sky modulation curve is subtracted from the target observation before further analysis.

3.1 Telescope polarization

All observations need to be corrected for TP. The TP is determined by observations of nearby stars that we believe to have very low polarization. The low-polarization calibrators were all stars we have used previously for this purpose with HIPPI (Bailey et al. 2015; Cotton et al. 2016a) or PlanetPol (Hough et al. 2006; Bailey et al. 2010). They are Sirius, β Leo (BS 4534), β Vir (BS 4540), β Hyi (HIP 2021, BS 98), and α Ser (BS 5854). Based on our previous observations of these objects, we believe they all have polarizations of ∼5 ppm or smaller.

We determined the TP separately for our blocks of observations in 2016 May and June, and July–September. The observations and adopted average TP values (in boldface) are listed in Table 2. The instrument was removed from the telescope and remounted and adjusted between each of these blocks. The TP adopted was the mean of the polarization of all calibrators observed within each block, and this was used to correct all other observations within the block.

When Sirius was observable, this was our preferred calibrator as it could be observed to a precision of usually better than 10 ppm in a short observation. The other objects were fainter, and typical precisions of individual observations were ∼20–30 ppm.

Between the May and June observing blocks, the instrument was modified by fitting with an improved aperture plate that removed some light leaks, and was remounted with a different orientation on the telescope. This probably explains the change in TP between these runs.

3.2 High-polarization stars

We have observed a number of high-polarization stars. These are used to calibrate the position angle of polarization and also provide a check on the efficiency calibration of the instrument. The stars observed and the parameters needed for our bandpass model are listed in Table 3.

These stars are distant stars polarized by the interstellar medium. The wavelength dependence of interstellar polarization can be represented by the empirical model (Serkowski, Mathewson & Ford 1975; Wilking et al. 1980)

$$P(\lambda) = P_{\max} \exp\left(-K \ln^2 \frac{\lambda}{\lambda_{\max}}\right), \quad (3)$$

where $P_{\max}$, $\lambda_{\max}$, and K are empirical parameters that are fitted to observed wavelength-dependent polarization measurements and are given in Table 3 for our standard stars. Since the wavelength dependence is well determined, we can calculate the polarization we expect to observe with Mini-HIPPI by integrating over the passband, as described by Bailey et al. (2015). The predicted polarizations are given in Table 3.

We observed HD 84810 on seven occasions, HD 147084 twice, and the other stars once. The average results are given in Table 3. It can be seen that the agreement between the predicted and observed polarization is excellent. The largest discrepancy between observed and predicted is 0.05 per cent for HD 154445. Other objects agree to 0.01–0.03 per cent. This is as good as can be expected considering the accuracy of the past results we are comparing with. The results demonstrate the accuracy of the instrument and of the bandpass model we are using to determine the efficiency corrections.

The position angles all agree with previous values to within 1°.

Table 2. Low-polarization star measurements to determine telescope polarization.

Block	Star	Date	P (ppm)	θ (°)
2016 May	Sirius	May 13	95.2 ± 7.8	93.2 ± 2.3
	Sirius	May 14	98.8 ± 8.3	91.9 ± 2.5
	Sirius	May 17	99.8 ± 8.2	90.6 ± 2.4
	Sirius	May 19	75.8 ± 8.7	83.0 ± 3.2
Average			**91.6 ± 4.1**	**90.1 ± 1.3**
2016 Jun	Sirius	June 9	62.1 ± 11.2	93.6 ± 5.5
	β Leo	June 9	67.5 ± 19.7	89.2 ± 8.4
	Sirius	June 10	54.2 ± 6.6	93.3 ± 3.6
	Sirius	June 15	61.3 ± 12.5	91.9 ± 6.0
	Sirius	June 16	57.2 ± 7.6	91.2 ± 3.7
Average			**60.4 ± 5.6**	**91.8 ± 2.7**
2016July–September	β Leo	June 29	31.7 ± 18.3	88.1 ± 16.2
	β Leo	June 29	83.8 ± 18.4	82.0 ± 6.4
	β Vir	June 29	116.9 ± 29.5	95.6 ± 7.3
	β Leo	July 1	64.4 ± 19.3	95.3 ± 8.2
	β Leo	July 1	59.8 ± 19.7	93.6 ± 9.6
	β Hyi	July 23	50.5 ± 26.7	93.0 ± 14.7
	β Hyi	July 23	89.4 ± 29.0	81.4 ± 19.3
	β Leo	July 24	101.1 ± 23.3	95.2 ± 6.5
	β Leo	July 25	32.9 ± 22.0	88.9 ± 19.0
	α Ser	August 11	89.4 ± 21.5	106.1 ± 6.8
	β Hyi	August 15	97.1 ± 19.3	108.5 ± 5.7
	β Hyi	August 31	77.8 ± 19.0	97.5 ± 7.0
	Sirius	September 19	59.3 ± 7.8	86.4 ± 4.1
	Sirius	September 19	83.0 ± 8.4	86.3 ± 3.2
Average			**71.0 ± 5.6**	**93.5 ± 2.3**

3.3 Comparison with other high-precision polarimeters

In Table 4, we compare Mini-HIPPI observations of a number of stars, most observed on multiple nights, with previous high-precision observations of these stars. Some of these earlier observations are with HIPPI on the AAT, either from Cotton et al. (2016a) or from new observations first reported here in the cases of ϵ Sgr and Acrux. Other observations are with PlanetPol on the William Herschel Telescope (Bailey et al. 2010). In making these comparisons, it is important to note that the wavelengths are not the same.

Table 3. Predicted and observed polarization for polarized standard stars.

Star	Spectral type	$E(B-V)$	R_V	P_{max}	λ_{max}	K	θ (°)	P (%)		θ (°)	References
								Predicted	Observed	Observed	
HD 84810	F8-K0Ib V	0.34	3.1	1.62	0.57	1.15	100.0	1.566	1.570 ± .002	99.9 ± 0.1	1, 2
HD 147084	A4 II/III	0.72	3.9	4.34	0.67	1.15	32.0	3.823	3.803 ± .005	31.8 ± 0.1	3, 4
HD 154445	B1V	0.42	3.15	3.73	0.558	0.95	90.1	3.576	3.629 ± .010	89.4 ± 0.1	1, 2, 3
HD 160529	A2 Ia	1.29	3.1	7.31	0.543	1.15	20.4	7.139	7.143 ± .022	20.8 ± 0.1	1, 2
HD 187929	F6-G0 I	0.18	3.1	1.76	0.56	1.15	93.8	1.696	1.684 ± .006	92.9 ± 0.1	1

References: (1) Serkowski et al. (1975); (2) Hsu & Breger (1982); (3) Wilking et al. (1980); (4) Martin, Clayton & Wolff (1999).

Table 4. Observations of low-polarization stars compared with HIPPI and PlanetPol observations.

Star	HD	Distance (pc)	Number of observations	Mini-HIPPI (350–700 nm)		HIPPI (400–550nm)		PlanetPol (590–1000nm)	
				P (ppm)	θ (°)	P (ppm)	θ (°)	P (ppm)	θ (°)
Sirius	48915	2.6	11	3.1 ± 2.7	8 ± 25	5.5 ± 1.7	114 ± 18		
β Hyi	2151	7.5	4	14.8 ± 11.5	127 ± 23	8.8 ± 2.5	95 ± 16		
β Leo	102647	11.1	7	11.8 ± 7.8	21 ± 19			2.3 ± 1.1	35 ± 14
Fomalhaut	216956	7.7	6	17.8 ± 5.9	73 ± 10	24.3 ± 3.1	111 ± 7		
Arcturus	124897	11.3	6	17.9 ± 4.4	7 ± 7			6.3 ± 1.6	31 ± 7
α Cen	128620/1	1.3	26	15.1 ± 1.9	34 ± 4				
Canopus	45348	94.8	6	122.8 ± 4.0	115 ± 1	112.8 ± 1.7	116 ± 1		
Acrux	108248	98.7	1	327.9 ± 14.1	114 ± 1	363.2 ± 1.7	113 ± 1		
ϵ Sgr	169022	43.9	2	112.7 ± 11.4	34 ± 3	115.3 ± 1.9	37 ± 1		

The HIPPI observations are in a narrower band, the Sloan Digital Sky Survey observations are in the g' band from about 400 to 550 nm, and the PlanetPol observations are in a much redder band from 590 to 1000 nm. The first three stars listed are stars that we use as low-polarization calibrators, so it is not surprising that the measured polarizations are low. The next three stars (Fomalhaut, Arcturus, and α Cen) are nearby bright stars that we are evaluating as potential bright low-polarization calibrators. Canopus is a somewhat more distant object that shows polarization, probably interstellar in origin. Acrux and ϵ Sgr (Cotton et al. 2016b) are B star systems that likely have both intrinsic and interstellar polarization contributions. It can be seen that the agreement between the Mini-HIPPI observations and earlier observations is typically at the ∼10 ppm level or better. Where there are somewhat larger differences, these are entirely consistent with plausible effects due to wavelength dependence.

At low levels of polarization where the polarization is of a similar magnitude to the error, observed values of polarization are subject to a positive bias (Simmons & Stewart 1985). Polarization data are sometimes corrected by applying a debiasing correction of which one common form is to replace P by $\sqrt{P^2-\sigma_P^2}$. Following our procedure in earlier publications (Bailey et al. 2010; Cotton et al. 2016a), we have not applied any debiasing correction to the data tabulated here. We apply such corrections only when they are needed for specific statistical analyses where the bias becomes important. We also note that in most cases the problem caused by this bias can be avoided by working in normalized Stokes parameters (Q/I and U/I) rather than in P and θ.

It can be seen from the results in Table 4 that Mini-HIPPI can easily detect polarization at levels ∼100 ppm, as shown by the results on Canopus and ϵ Sgr, which agree very well in polarization and position angle with previous observations. In principle, the detection of polarization levels down to ∼20 − 30 ppm should be possible, but this is hard to test with the limited existing data on polarization at these levels.

It should be noted that Arcturus is reported by Kemp et al. (1986) to be a polarimetric variable with an amplitude of about 50 ppm in the B band and a possible period of around 45 d. Our current observations are insufficient to confirm such variability.

Our observations of α Cen apply to the combined light of both α Cen A and B. Although α Cen was previously observed by HIPPI (Cotton et al. 2016a), the observation is considered unreliable because α Cen B would have been close to the edge of the aperture.

3.4 Performance versus magnitude

In Fig. 6, we have plotted the polarization errors derived from the data reduction system for a range of stars observed with Mini-HIPPI against the B magnitude of the stars. The measured errors have been scaled to a uniform integration time (T) of 1000 s under the assumption that the error scales as $T^{-0.5}$. The actual integration times ranged from 400 to 1600 s. Over most of the range, it can be seen that the error scales with magnitude in the way expected for photon-shot-noise-limited performance, as shown by the line in the diagram. However, the performance is relatively poorer (above the line) for the brightest stars. This could be an indication that the 500-Hz modulation we are using is not fast enough to completely remove scintillation noise for the brightest stars. It may also be in part due to the requirement to turn down the PMT gain by using a lower HT voltage to avoid saturation for these stars. The dashed line on the diagram shows the performance expected for Mini-HIPPI on a 1-m telescope.

3.5 Observations of Spica

As an example of the type of science that can be done with Mini-HIPPI, we present observations of Spica (α Vir). Spica is a binary system consisting of two B stars orbiting with a period of just over 4 d. Previous polarimetry of Spica was presented by Pfeiffer & Koch (1977), who described it as unpolarized and gave a value of $P = 0.03 \pm 0.01$ per cent. Tinbergen (1982) reported observations showing

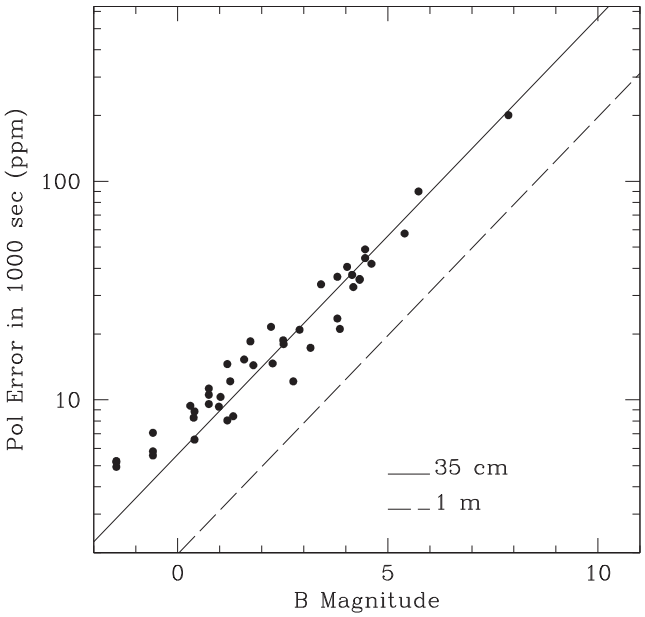

Figure 6. Polarization errors of Mini-HIPPI observations scaled to 1000-s integration and plotted against B magnitude. The line has the slope expected for photon-noise-limited performance and is fitted through the points for the fainter stars. The dashed line is the expected performance for Mini-HIPPI on a 1-m telescope.

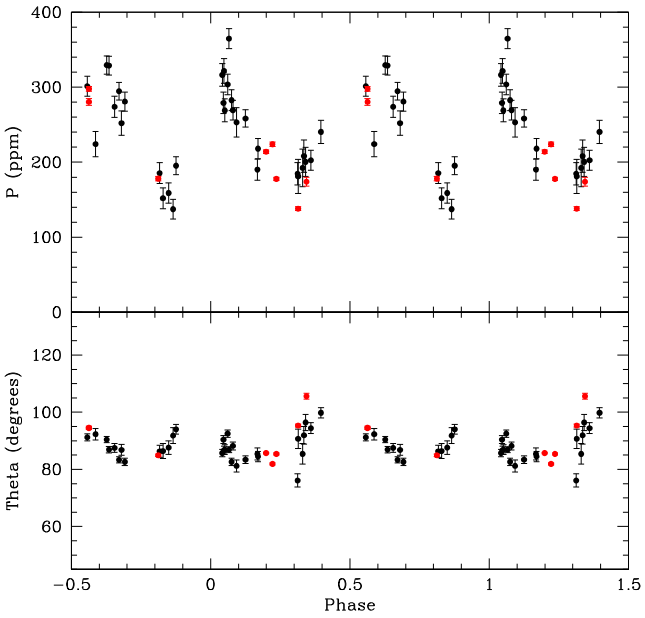

Figure 7. Mini-HIPPI observations (in black) of the polarization and position angle of Spica plotted against phase on the orbital period. The red points are observations of Spica in the g' band taken with HIPPI on the AAT.

a marginal detection of polarization in the Q Stokes parameter. Elias, Koch & Pfeiffer (2008) also report a small polarization in an average of 11 measurements but say that the standard deviation indicates that this star is not a polarization variable. Cotton et al. (2016a) presented three measurements of Spica with HIPPI on the AAT that showed clear polarization and significant variability.

In Fig. 7, observations of Spica obtained with Mini-HIPPI show clear periodic variability in polarization and position angle. The observations are plotted against phase on the orbital cycle according to the ephemeris of Tkachenko et al. (2016). Zero phase corresponds to the time of periastron passage.

Also plotted in Fig. 7 are eight observations of Spica obtained with HIPPI on the AAT in the g' band. Although this is a different band from the one used for Mini-HIPPI, the effective wavelengths are similar. It can be seen that the HIPPI and Mini-HIPPI observations appear quite consistent.

These results show that Mini-HIPPI, even on a very small telescope, is capable of easily detecting polarization variation, whereas that was not detectable with a previous generation of polarimeters.

We are continuing to monitor the polarization of Spica with the aim of filling in the remaining gaps in the phase curve, and we will present a full analysis at a later date. Spica is an important system because it enables the polarimetric modelling of a binary system to be compared with the results of interferometric observations (Herbison-Evans et al., 1971).

4 CONCLUSIONS

We have described the Mini-HIPPI polarimeter, a compact and lightweight instrument, based on the use of an FLC modulator. Test observations with Mini-HIPPI on a 35-cm telescope show polarizations for standard stars in excellent agreement with predicted values. We measure the telescope polarization to be ∼60–90 ppm. A number of stars observed with Mini-HIPPI show polarization results typically within about 10 ppm or better of previous measurements with other high-precision polarimeters. We have used Mini-HIPPI to study the polarization of the binary star system Spica, and it easily detects periodic polarization variations around the binary cycle, which were not detectable with the precision available on earlier instruments.

ACKNOWLEDGEMENTS

This work was supported by the Australian Research Council through Discovery Projects grant DP 160103231.

REFERENCES

Bailey J., Lucas P. W., Hough J. H., 2010, MNRAS, 405, 2570
Bailey J., Kedziora-Chudczer L., Cotton D. V., Bott K., Hough J. H., Lucas P. W., 2015, MNRAS, 449, 3064
Bott K., Bailey J., Kedziora-Chudczer L., Cotton D. V., Lucas P. W., Marshall J. P., Hough J. H., 2016, MNRAS, 459, L109
Castelli F., Kurucz R. L., 2004, preprint (arXiv:astro-ph/0405087)
Cotton D. V., Bailey J., Kedziora-Chudczer L., Bott K., Lucas P. W., Hough J. H., Marshall J. P., 2016a, MNRAS, 455, 1607
Cotton D. V., Marshall J. P., Bott K., Kedziora-Chudczer L., Bailey J., 2016b, in Short W., Caprarelli G., eds, Proc. 15th Aust. Space Res. Conf., National Space Society of Australia, Sydney, p. 55
de Juan Ovelar M., Diamantopoulou S., Roelfsema R., van Werkhoven T., Snik F., Keller C., 2012, in Angeli G. Z., Dierickx P., eds, Proc SPIE Conf. Ser. Vol. 8449, Modelling, Systems Engineering and Project Management for Astronomy V. SPIE, Bellingham, p. 844912
Elias N. M., Koch R. H., Pfeiffer R. J., 2008, A&A, 489, 911
Gisler D., Feller A., Gandorfer A., 2003, in Fineschi S., ed., Proc SPIE Conf Ser. Vol. 4843, Polarimetry in Astronomy. SPIE, Bellingham, p. 45
Herbison-Evans D., Hanbury-Brown R., Davis J., Allen L. R., 1971, MNRAS, 151, 161
Hough J. H., Lucas P. W., Bailey J. A., Tamura M., Hirst E., Harrison D., Bartholomew-Biggs M, 2006, PASP, 118, 1302
Hsu J., Breger M., 1982, ApJ, 262, 732
Kemp J. C., 1969, JOSA, 59, 950
Kemp J. C., Barbour M. S., 1981, PASP, 93, 521

Kemp J. C., Henson G. D., Kraus D. J., Beardsley I. S., Carroll L. C., Duncan D. K., 1986, ApJ, 301, L35
Kemp J. C., Henson G. D., Steiner C. T., Powell E. R., 1987, Nature, 326, 270
Lucas P. W., Hough J. H., Bailey J. A., Tamura M., Hirst E., Harrison D., 2009, MNRAS, 393, 229
Marshall J. P. et al., 2016, ApJ, 825, 124
Martin P. G., Clayton G. C., Wolff M. J., 1999, ApJ, 510, 905
Pfeiffer R. J., Koch R. H., 1977, PASP, 89, 147
Sabatke D. S., Descour M. R., Dereniak E. L., Sweatt W. C., Kemme S. A., Phipps G. S., 2000, Opt. Lett., 25, 802
Serkowski K., Mathewson D. S., Ford V. L., 1975, ApJ, 196, 261
Simmons J. F. L., Stewart B. G., 1985, A&A, 142, 100
Tinbergen J., 1982, A&A, 105, 53.
Tkachenko A. et al. 2016 MNRAS 458, 1964
Wiktorowicz S. J., Matthews K., 2008, PASP, 120, 1282
Wiktorowicz S., Nofi L. A., 2015, ApJ, 800, L1
Wiktorowicz S., Nofi L. A., Daniel J.-T., Kopparla P., Laughlin G. P., Hermis N., Yung Y. L., Swain M. R., 2015, ApJ, 813, 48
Wilking B. A., Lebofsky M. J., Martin P. G., Rieke G. H., Kemp J. C., 1980, ApJ, 235, 905

This paper has been typeset from a TEX/LATEX file prepared by the author.